A Facile Temperature-Controlled "Green" Method to Prepare Multikinds of High-Quality Alumina Hydrates via a Ga-In-Sn-Alloyed Aluminum−Water Interface Reaction

Wenjing Fu, Cundi Wei, Jing Zuo, Jiupeng Zhang, Jinyi Zhang, and Shaonan Xu*

Read Online

ACCESS | Metrics & More | Article Recommendations | SI Supporting Information

ABSTRACT: The Al sheets alloyed by Ga-In-Sn are generally utilized to react with water for H_2 production, while the valuable byproducts, *i.e.*, alumina hydrates, have not been fully studied. In this work, through controlling the reaction temperature, three types of alumina hydrates, bayerite (40 °C), pseudo-boehmite (PB) (70−120 °C), and boehmite (130−160 °C), were successfully prepared based on a series of interface reactions and structural transformations. These alumina hydrates and their calcined products (alumina) possess high purity with a total impurity element content of <450 ppm, especially an extremely low sodium content (<21 ppm) and iron content (<52 ppm). Significantly, the obtained pseudo-boehmite displays excellent surface properties (specific surface area: 332.7 m^2 g^{-1}, pore volume: 0.3 cm^3 g^{-1}, and pore diameter: 3.6 nm), competitive to the current commercial SB powder by Sasol. This work not only deepens the understanding of the byproducts in a Ga-In-Sn-alloyed Al−water reaction but also establishes a facile "green" method oriented to industrial applications, which is promising for the linkage benefits of the hydrogen production industry.
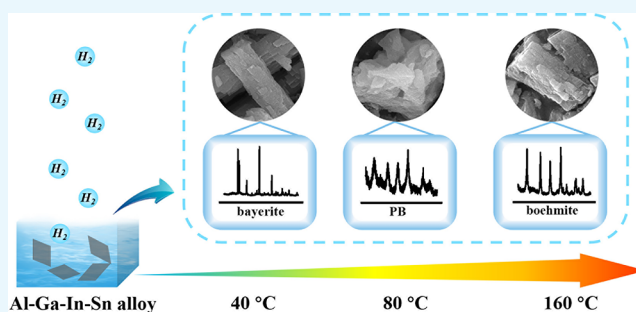
1. INTRODUCTION

A Ga-In-Sn-alloyed Al−water reaction, as a typically effective way to produce hydrogen (H_2), has been broadly utilized to store hydrogen energy in a solid state with safety, controllability, and convenience.[1,2] However, this approach is burdened with the relatively high cost in preparing the Ga-In-Sn-Al raw materials, which limits its further industrial applications.[3] In general, two different approaches had been utilized to relieve this dilemma. One effort is paid to pursue a better performance on hydrogen production,[4,5] while the other one focuses on the reutilization of the byproducts of the reactions, rather than handling them as solid wastes. However, to date, there are few reports available on the systematic investigation of the specific types of solid byproducts in this reaction, let alone their full reutilization.

The conventional opinion generally holds that the solid byproducts of the reaction (Ga-In-Sn-Al alloy with water) mainly consist of alumina hydrates—bayerite, *i.e.*, Al $(OH)_3$.[6] Recently, it has been reported that other more valuable alumina hydrates, such as gibbsite and boehmite, can also be obtained by adding alditols and seed.[7,8] Owing to the versatile crystal types and excellent physical and chemical properties, alumina hydrates (usually referred to as $Al_2O_3 \cdot nH_2O$, contains bayerite, pseudo-boehmite (PB), boehmite, and so on), together with their calcined products (alumina), have remarkable economic value in the diverse application fields of catalysts, catalyst supports,

ceramics, adsorbents, and coatings,[9−15] especially catalysis, which has become an important direction of chemical industry development.[16−20] It is also worth pointing out that, so far, the commonly used methods to prepare bayerite, PB, and boehmite generally include the Bayer method, hydrothermal/precipitation method, and aluminum alkoxide method.[21−26] However, they are usually burdened with complex processes and various chemicals.[27−29] In addition, to the best of our knowledge, few of them have a close connection with the recycling of the byproducts from hydrogen production (*i.e.*, from a Ga-In-Sn-alloyed Al−water reaction).

Here in this work, we made progress in recycling the byproducts of the Ga-In-Sn-alloyed (Ga: 1.34 wt %, In: 0.41 wt %, and Sn: 0.25 wt %) Al−water reaction, where three different alumina hydrates (*i.e.*, bayerites, PB, and boehmite) were obtained via a facile method, *i.e.*, controlling the reaction temperature. Furthermore, these byproducts were proven to have satisfactory purity and surface properties (*e.g.*, PB has a specific surface area of 332.7 $m^2 g^{-1}$, pore volume of 0.3 $cm^3 g^{-1}$,

and pore diameter of 3.6 nm), which can directly meet the requirements of the industrial standard (competitive to its commercial counterpart SB powder by Sasol). Our results not only enriched the systemic understanding toward the aluminum–water reaction but also constructed a facile way to produce a series of high-purity alumina materials. Moreover, this approach has more superiority in industrial applications due to the relatively high purity of the products, less introduction of chemicals, environmentally friendly preparation process, and additional benefits toward the hydrogen production industry.

2. EXPERIMENTAL SECTION

2.1. Materials. All raw materials used for alloy preparation were used directly in this work without any further purification. The Al sheets used in this experiment are composed of Al (98 wt %), Ga (1.34 wt %), In (0.41 wt %), and Sn (0.25 wt %). The SB powder (pseudo-boehmite produced by Sasol, mass fraction ≥ 99.9%) was purchased from Yangzhou Zhongtianli Company. Deionized water was used for all syntheses and treatment processes. The detailed information of the metal reagents is presented in Table 1.

Table 1. Description of Metal Reagents

reagents	CAS No.	mass fraction	suppliers
gallium (Ga)	7440-55-3	99.99%	Aladdin
indium (In)	7440-74-6	99.995%	Aladdin
stannum (Sn)	7440-31-5	99.5%	Aladdin
aluminum (Al)	7429-90-5	99.99%	Beijing Xingrongyuan Technologgy Co., Ltd

2.2. Synthesis of Different Phases. The Al sheets were prepared by melting different proportions of metals (Al, Ga, In, and Sn) at a high temperature (800 °C) for 2 h under a nitrogen atmosphere. After rapidly cooling down, the alloy ingot was obtained and then processed into sheets to increase the reaction contact area. Afterward, the Al sheets were immersed in 3 L of distilled water heated to a particular temperature (40–160 °C) in a high-pressure reactor with a solid:liquid ratio of 1:100 (g/mL). During the reaction, hydrogen was produced and collected for further utilization. After that, the suspending slurry obtained was filtered and dried at a temperature of 80 °C for 12 h to obtain alumina hydrates while the bottom residue consisting of the remaining Al with Ga, In, and Sn was recycled. Different crystal forms of alumina were obtained by calcination of alumina hydrates under various temperatures (300/550/800/1000/1200 °C).

2.3. Characterization. X-ray diffraction (XRD) was performed using a DX2700 diffractometer with a Cu Kα radiation source (λ = 1.5406) in a 2θ range from 5 to 80°. The Fourier transform infrared spectra (FTIR) were collected on a Bruker IFS 66v/s spectrometer, which was operated between 4000 and 500 cm^{-1} with 128 scans per spectrum. Scanning electron microscopy (SEM) tests were performed on a JEOL JSM-6700F microscope to reveal the morphology of the synthesized samples. The specific surface area data and pore size distribution were obtained from a JW-BK222 automated sorption system by using the Brunauer–Emmet–Teller (BET) model and the Barret–Joyner–Halenda (BJH) model, respectively, and all samples were degassed at 150 °C for 4 h prior to the measurements. Transmission electron microscopy

(TEM) and high-resolution TEM (HRTEM) characterizations were performed with a JEOL JEM-2100F microscope at an acceleration voltage of 200 kV. Inductively coupled plasma-mass spectrometry (ICP-MS) analysis was conducted on a HORIBA ICP-optical emission spectrometer. (The ICP-MS test process is as follows: Taking element Ga as an example, with the estimation of about 1 mg of Ga element, a certain corresponding amount of sample was weighed and dissolved with dilute nitric acid. After the sample was completely dissolved, the solution volume was adjusted to 1 L and 100 mL of the solution was taken for the ICP-MS test. Then, the mass fraction of Ga element in the corresponding sample can be obtained. The testing procedure for other elements is the same as that for Ga element.). TG-DTA characterization was performed with HCT-3 microcomputer differential thermal balance with a heat rate of 10 °C/min produced by Beijing Hengjiu Scientific Instrument Factory.

3. RESULTS AND DISCUSSION

3.1. Analysis of Raw Materials. First, we characterize the phase composition and morphology of Al alloy sheets. As shown in Figure 1 (inset), the SEM image indicates that the alloy sheets
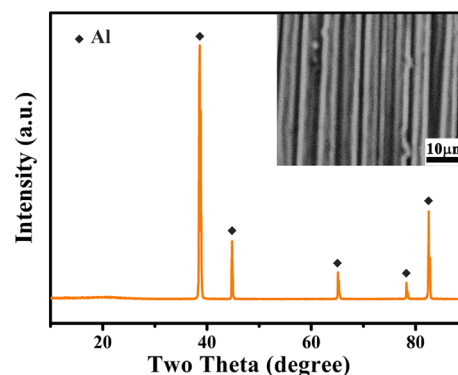

Figure 1. X-ray diffraction pattern and SEM image (inset) of an Al alloy piece.

present a slender rod-like structure with a width between 2 and 5 μm. From the X-ray diffraction pattern (Figure 1), only the peaks of Al phase (JCPDS file #04-0787) can be observed, whereas the characteristic peaks of any phase structures consisting of Ga, In, and Sn cannot be detected. It indicates that the addition of Ga, In, and Sn is considerably low.

3.2. XRD and FT-IR Characterizations of the By-products. Next, we monitored the evolution of the solid byproducts (obtained from different reaction temperatures, within the range 40–160 °C). As shown in Figure 2a,b, through comparing with the standard cards of bayerite, PB, and boehmite materials, the XRD results indicate that there are four stages in the evolution (also labeled in Table 2): (1) at a relatively low reaction temperature (i.e., 40 °C), only the high-purity bayerite can be observed; (2) with the temperature increasing to 50–60 °C, the appearance of new peaks indicates the existence of a mixed phase (bayerite and PB); (3) at 70–120 °C, diffraction peaks of bayerite no longer exist and the pure PB phase is formed; (4) at 130–160 °C, with the improvement of crystallinity (which can be confirmed by the more sharpened diffraction peaks), the appearance of new peaks (45.8, 51.7, and 53°), and the separation of the peak at 64° into two smaller peaks, pure boehmite is observed.[30] In addition, we calculated
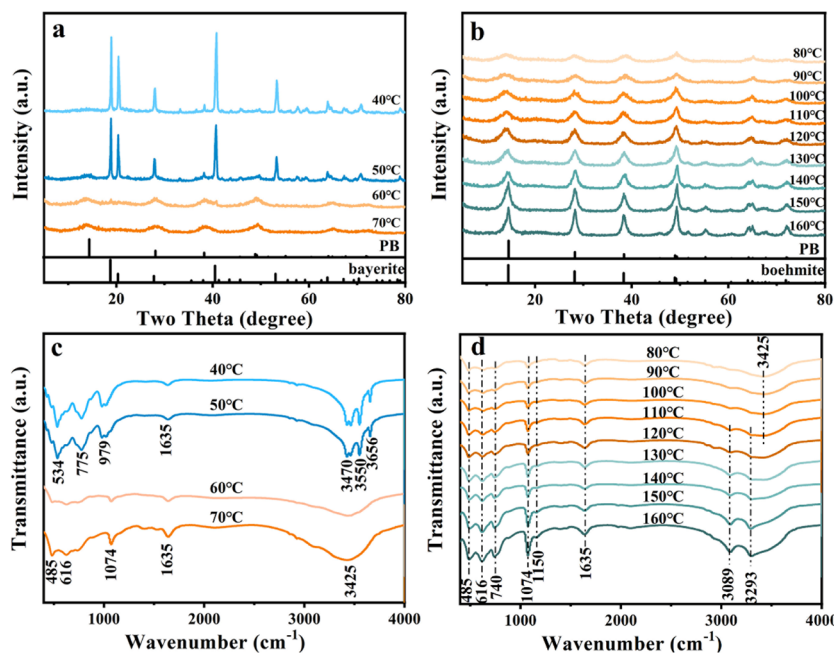
Figure 2. (a, b) X-ray diffraction patterns of the series samples (prepared from 40 to 160 °C). (c, d) FT-IR spectra of the series samples (prepared from 40 to 160 °C).

Table 2. Four Different Stages in the Temperature-Dependent Reactions

temperature	corresponding reactions
40 °C	$2Al + 6H_2O \rightarrow 2Al(OH)_3$ (bayerite) $+ 3H_2\uparrow$
50−60 °C	$2Al + 6H_2O \rightarrow 2Al(OH)_3$ (bayerite) $+ 3H_2\uparrow$; $2Al + 4H_2O \rightarrow 2AlOOH$ (PB) $+ 3H_2\uparrow$
70−120 °C	$2Al + 4H_2O \rightarrow 2AlOOH$ (PB) $+ 3H_2\uparrow$
130−160 °C	$2Al + 4H_2O \rightarrow 2AlOOH$ (boehmite) $+ 3H_2\uparrow$

the MCD (microcrystalline dimension) value along the specific crystal plane ((100) for bayerite and (020) for PB and boehmite) (shown in Figure S1). The results show that the MCD value of bayerite obtained at 40 °C is 33.8 nm and, with the temperature increasing up to 70 °C, the variation of MCD shows positive correlations with temperature, indicating the steady growth of the crystals from 2.5 to 7.5 nm along with the direction of (020). This result indicates that the transformation process of PB to boehmite is gradual.

Similar results can also be obtained from the FT-IR testing (Figure 2c,d). The characteristic peaks of the Al−OH bond of bayerite (stretching vibration) at 3470, 3550, and 3656 cm⁻¹ disappear at 60−70 °C, which confirms the bayerite → PB phase transition.[31,32] Above 70 °C (up to 160 °C), there is no appreciable change in the position of IR peaks between 400 and 2000 cm⁻¹. The peaks at 485, 616, and 740 cm⁻¹ belong to the AlO₆ vibrations, while the peaks at 1070 and 1150 cm⁻¹ belong to the Al-OH bending vibrations. The peak at 1635 cm⁻¹ existing under various temperature conditions is assigned to the H-O-H bending mode, which represents the physically adsorbed water. However, the absorption peaks in the wavenumber range of 3000 to 4000 cm⁻¹ (3089, 3293, and 3425 cm⁻¹), which represent the different Al-OH stretching vibrations, have presented a relatively obvious change. At 70 °C, there is only one broad absorption peak at 3425 cm⁻¹, whereas two obvious symmetrical peaks appeared (3089 and 3293 cm⁻¹) when the temperature is gradually increased to 160 °C from 110 °C, indicating a typical PB → boehmite phase transition.[33,34] In

view of the above analysis, a brief summary is displayed in Table 2, in which the specific changes in the production phase as the reactive temperature increases are clearly observed.

3.3. Microstructure (SEM and TEM) Analysis of the Three Alumina Hydrates. The surface morphology of the samples prepared under different hydrothermal temperatures is characterized by SEM and TEM. Consistent with the typical morphology features of bayerite shown in the literature,[35] the bayerite obtained at 40 °C presents an hourglass-like structure. As shown simultaneously in Figure 3a,d, the bayerite crystals are obviously formed by the stack of various plates along a certain direction, giving the appearance of an elongated shape. The HRTEM image (Figure 3g) reveals the clear lattice fringes with a spacing of 0.236 nm, which is consistent with that of the (002)
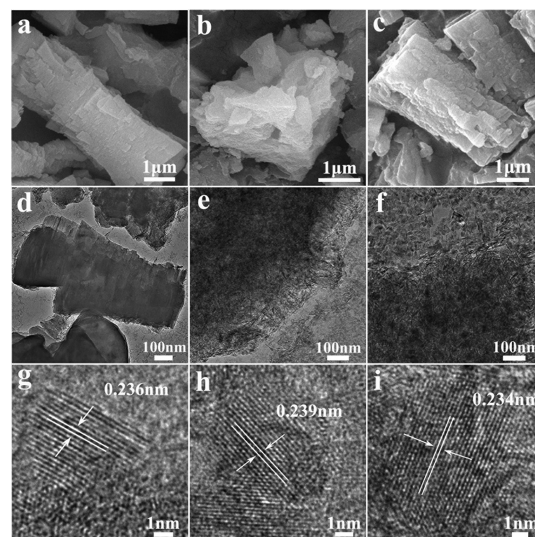

Figure 3. SEM, TEM, and HRTEM images of the three alumina hydrates: (a, d, g) bayerite prepared at 40 °C, (b, e, h) PB prepared at 80 °C, and (c, f, i) boehmite prepared at 160 °C.

plane of bayerite. The PB prepared at 80 °C displays a similar plate-stacking structure to the bayerite and forms an irregularly shaped stacked structure. In addition, the TEM image in Figure 3e displays the relatively numerous fibrillar structures, indicating the thinner plate structure of PB. Interestingly, the boehmite formed at 160 °C has a structure similar to bayerite, which can be roughly regarded as a half-hourglass shape or cuboid shape. Meanwhile, the more regular morphology of boehmite shown in Figure 3c together with the obvious fibrillar and sheet structure appearing concurrently in Figure 3f reveals a significant improvement in crystallinity (compared with PB obtained at 80 °C), which agrees well with the result of the X-diffraction pattern. The HRTEM image (Figure 3i) elucidates the lattice fringes with a spacing of 0.234 nm, corresponding to the (031) plane of boehmite. Meanwhile, the PB obtained presents a larger lattice spacing of 0.239 nm (corresponding to the (031) plane) due to the extra water in an interlaminar structure (Figure 3h). In spite of displaying different morphological characteristics, the plate-stacking structure exists in all three hydrates (as shown in Figure 3a−c) due to the fact that the plates (formed by two-dimensional growth after the nucleation) impinge upon each other with their increase in number and thickness as the reaction proceeds.[36]

3.4. Formation Mechanism Analysis of the Three Alumina Hydrates.
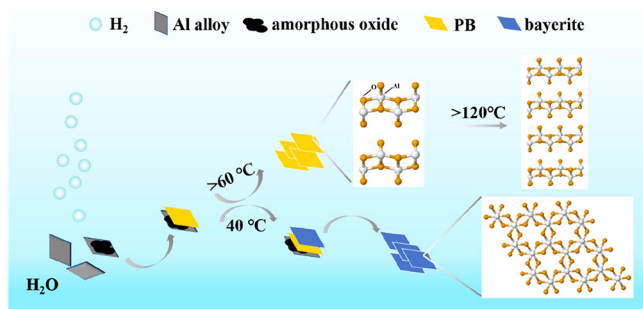The possible reaction mechanism is illustrated in Figure 4. The formation of the final phase of the

Figure 4. Interface reactive process of Al with water at different reaction temperatures.
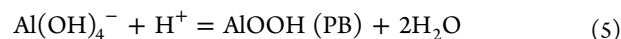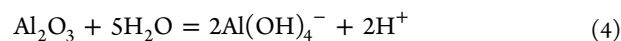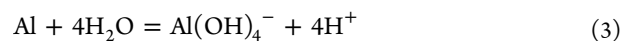
product depends on the synergistic effect of pH and temperature. However, in this work, the initial pH value of the reaction is the same in the preparation of the three alumina hydrates, which are all around 7. The influence of pH on the product phase in the acid method (reaction of aluminum nitrate with ammonia) is discussed in the literature,[12] and it is proven that

both PB and bayerite can be generated under the condition of pH = 7. Therefore, in this work, the regulation of temperature is more decisive for the final phase type of the product.

There are two main stages in our reaction,[37−40] i.e.,

(1) direct dissolution of Al as well as the formation and dissolution of amorphous oxide;

(2) the precipitation of the hydrous oxide.

According to the kinetics theory, PB is the most accessible product. The whole process can be represented by the following reactions:[36,41]

$$Al + 4H_2O = Al(OH)_4^- + 4H^+ \tag{3}$$

$$Al_2O_3 + 5H_2O = 2Al(OH)_4^- + 2H^+ \tag{4}$$

$$Al(OH)_4^- + H^+ = AlOOH \ (PB) + 2H_2O \tag{5}$$

However, under a relatively low reaction temperature (e.g., 40 °C), the initially formed PB has numerous defects and pores and poor crystallinity, thus possessing a higher solubility than bayerite. Therefore, it will dissolve quickly and tend to re-crystallize to form bayerite on the surface of the crystal.[42] Since the stages (1) and (2) occur ceaselessly with time elapsing, the PB → bayerite transition can be repeated continuously, resulting in the accumulation of pure bayerite.

On the other side, with respect to the situation at the reaction temperatures over 70 °C, the significantly improved crystallization enables the initially formed PB to "survive" from the self-dissolution process,[39] contributing to the continuous crystal growth of PB. Since boehmite requires a higher formation temperature,[43] pure PB can be obtained within a temperature range of 70−120 °C, while a well-crystallized pure boehmite can be obtained via PB → boehmite transition over 130 °C. It is worthy to notice that the multi-step interface reaction process occurs at a relatively high speed in our work. This is because a certain amount of low-melting-point Ga-In-Sn alloy was incorporated into the Al sheets by high-temperature melting, resulting in the surface oxide layer being destroyed, which provides a favorable condition for the rapid process of reaction.[44,45] Therefore, when the reaction time was 5 h, the hydrates that we obtained were all the final products with pure phase, instead of intermediate products. In addition, the yield of each product can reach to 87% (bayerite), 93% (PB), and 97% (boehmite), respectively (shown in Table S1), which is conducive to actual industrial production.

3.5. Purity Analysis of the Three Alumina Hydrates.
To confirm the purity of our products, we performed ICP-MS measurement on the obtained bayerite (40 °C), PB (80 °C),
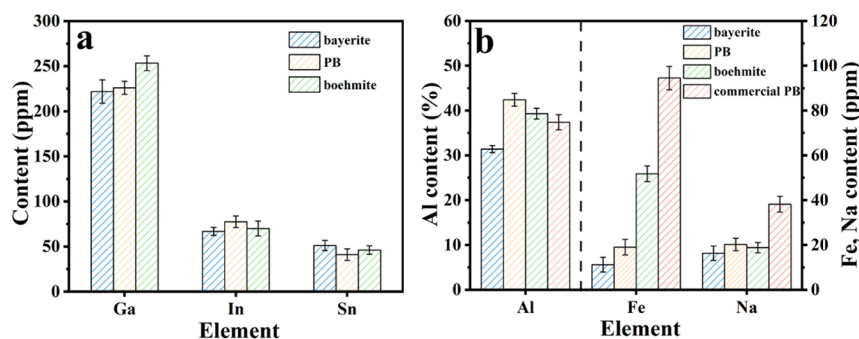

Figure 5. ICP-MS analysis of the three alumina hydrates (40 °C-bayerite, 80 °C-PB, and 160 °C-boehmite): (a) Ga, In, and Sn element contents of the three alumina hydrates and (b) comparison of Al, Fe, and Na contents of the three alumina hydrates and commercial PB (SB, produced by Sasol).
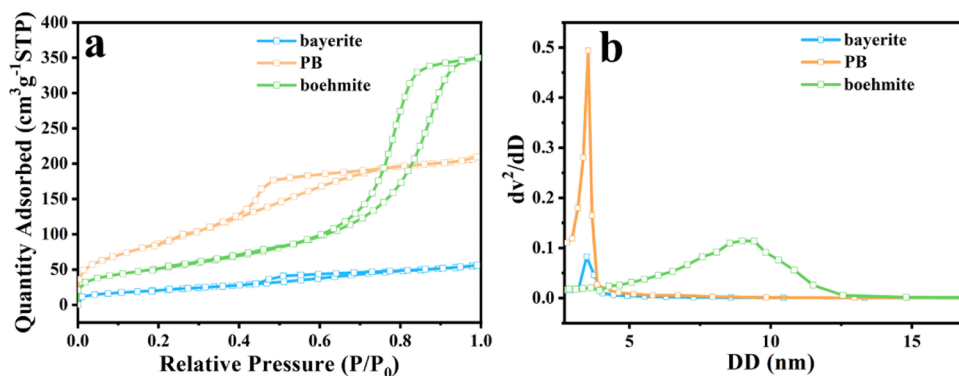
Figure 6. (a) N_2 adsorption−desorption isotherms and (b) pore size distribution for the three alumina hydrates (40 °C-bayerite, 80 °C-PB, and 160 °C-boehmite) (based on a Barret−Joyner−Halenda model).

boehmite (160 °C), and commercial PB. As shown in Figure 5a,b, the main impurity elements contained in our samples display only extremely low amounts (the sum is less than 450 ppm, the specific data is shown in Table S2), especially the Na impurity (<21 ppm) and Fe impurity (<52 ppm), while the Fe/Na impurity content of commercial PB is much higher than that of the alumina hydrates prepared in this work, which is shown in Figure 5b. Generally speaking, when alumina hydrates are used as catalysts or catalyst carriers, the presence of sodium and iron will poison the catalysts and severely reduce the catalytic performance, which will hinder the applications of alumina hydrates in the field of catalysis.[46,47] This advantage highlights our method from the most commonly used carbonization method (via the reaction of $NaAlO_2$ and CO_2) and the Bayer method. In addition, the low doped Ga/In/Sn impurities (shown in Figure 5a) play the role of catalysts, which are not involved in the reaction directly.[46] Therefore, they can be easily recycled by centrifugation (together with the aluminum residue). In that case, the purity of our samples can be further improved.

3.6. Surface Property Analysis of the Three Alumina Hydrates. Utilization in the catalyst field is a significant application of alumina hydrates, which usually requires them to have a relatively large specific surface area.[48] To confirm the potentiality of our products, we measured the nitrogen adsorption−desorption isotherms and pore size distribution curves of our samples. As shown in Figure 6 and Table 3, all the

Table 3. Surface Properties of the Three Alumina Hydrates Prepared at Different Temperatures

alumina hydrates	specific surface area ($m^2\,g^{-1}$)	pore volume ($cm^3\,g^{-1}$)	pore diameter (nm)
40 °C-bayerite	76.5	0.1	4.1
80 °C-PB	332.7	0.3	3.6
160 °C-boehmite	187.6	0.5	8.2

synthetic samples exhibit type IV isotherms with the hysteresis loop, which indicates the existence of a mesoporous structure.[49,50] According to the SEM image in Figure 3, it can be inferred that the mesopore structure is derived from the interspace formed by the stacking of the thin plate. Specifically, boehmite (prepared at 160 °C) shows a well-developed H1-shaped hysteresis loop, corresponding to the presence of cylindrical pores. The other two samples exhibit a typical H2-shaped hysteresis, which is a typical character of ink-bottle pores.[51] In addition, the bayerite (prepared at 40 °C) exhibits

the poorest adsorption volume, i.e., the smallest surface area ($76.5\,m^2\,g^{-1}$) and pore volume ($0.1\,cm^3\,g^{-1}$), while in PB (prepared at 80 °C), the pore diameter is moderately enlarged, which can be confirmed from the shifting of the hysteresis loop (move to a relatively high-pressure region). As for the boehmite, the closure points of the loop occurred at the region of $P/P_0 >$ 0.9, indicating the presence of the largest pore size as well as a broadened size distribution of pores (from 2.5 to 12.5 nm, shown in Figure 6b).[52] Furthermore, it is worth noticing that the parameter of the specific surface area is decreased in the PB → boehmite transition, which can be explained by the merging of the relatively small pores during the reaction and the enlarged grain size. Finally, we compared the optimized sample in our reaction (i.e., PB prepared at 80 °C) with several reported materials. As shown in Table 4, it is quite gratifying to find out that the properties of our product are fully comparable with other competitors, even competitive with the commercial material (SB produced by Sasol).

3.7. Thermal Analysis (TG-DTA) and Analysis of Calcined Products (Al_2O_3). Importantly, the calcined products of alumina hydrates, aluminas, with different crystal forms are widely used in industrial catalysis because of their excellent physical and chemical properties. Therefore, we carried out the thermal analysis of alumina hydrates and calcined them at different temperatures. As shown in Figure 7a,c,e, the DTA peaks observed at <100 °C of all three samples indicate the removal of physically adsorbed water. In Figure 7a, the DTA peak around 300 °C corresponds to the dihydroxylation of bayerite with a weight loss of 27% and then to transition alumina with a final weight loss of 39.5%, which is only slightly higher than the theoretical value of 34.6%.[12] Unlike in the bayerite, an obvious DTA peak occurs at a temperature of 400−500 °C in both PB and boehmite, which corresponds to the formation of γ-Al_2O_3 (Figure 7b,c).[58] Compared with boehmite, a continuous weight loss in PB can be observed at the temperature range from 150 to 430 °C, revealing the gradual dehydration of hydroxyl water. The total weight loss of boehmite is 25.3%, while there is a higher weight loss of 31.8% in PB because of the excess water it contained.[59] The results above show that the thermal properties of our as-obtained samples are consistent with those of the typical bayerite, PB, and boehmite, which indicates that they are suitable for calcination.

Finally, we investigate the derivatives of the synthesized products—aluminas. Generally, the transformation processes depend on the species of hydrates. Typically, for the bayerite (Figure 7b), the mixture phase of boehmite and η (η-Al_2O_3) is

Table 4. Comparison of the Surface Properties of PB (Prepared at 80 °C) from Previous Reports and Our Results

| methods	specific surface area ($m^2 \, g^{-1}$)	pore volume ($cm^3 \, g^{-1}$)	pore diameter (nm)	references
reaction-crystallization	342	0.53	3	53
hydrothermal synthesis	225.4	0.4	3.5	54
sol−gel	264.6	0.47	2.13	55
hydrothermal synthesis (with Brij 56 as a surfactant)	381	0.6	3	56
precipitation method with three kinds of surfactants (CTAB/TritonX-100/AOT)	297.3	0.41	5.2	49
	296.8	0.40	5.4	
	296.3	0.36	4.1	
sol−gel	231	0.28	4.52	57
hydrolysis of aluminum alkoxide	244.5	0.38	4.92	SB (Sasol)
reaction of Al-H_2O	332.7	0.3	3.6	this study (PB)
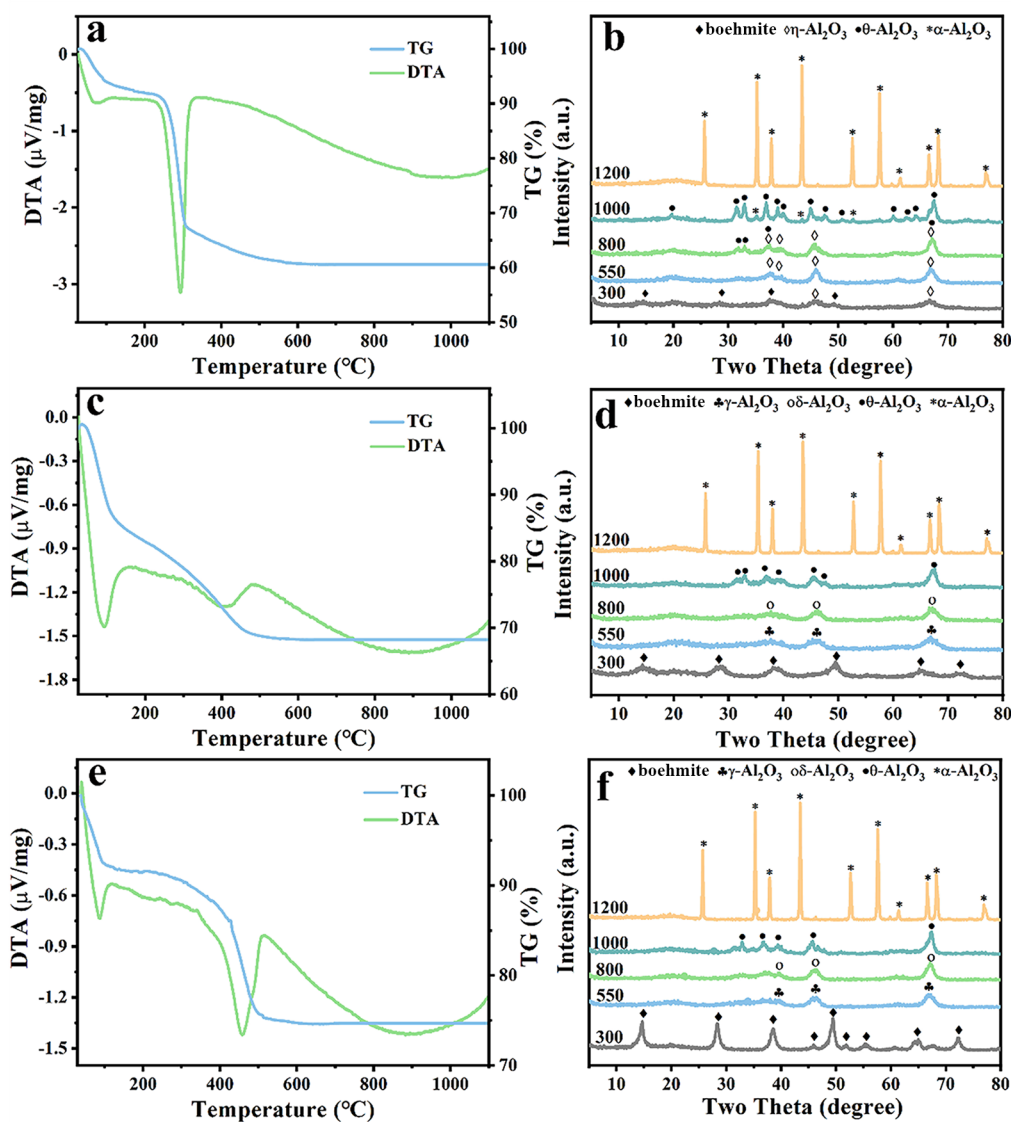
Figure 7. (a, c, e) Thermal analysis plots (DTA and TG) of the three alumina hydrates: (a) 40 °C-bayerite, (c) 80 °C-PB, and (e)160 °C-boehmite. (b, d, f) Series of XRD patterns of the products obtained by calcining (b) bayerite, (d) PB, and (f) boehmite under different temperatures (°C) for 3 h.

obtained at 300 °C, which well agrees with the results of the TG-DTA experiment (Figure 7a). When the temperature reaches 550 °C, the pure η phase can be observed. Further increasing the temperature to 800 °C ($\eta + \theta$) and 1000 °C ($\theta + \alpha$), the products return to the mixtures. Last, the pure α phase product is obtained at 1200 °C. On the other hand, for both PB (Figure 7d)

and boehmite (Figure 7f), no mixture phase composition can be observed at 300 °C, and the only difference is the slightly varied crystallinity. The first modification phase is obtained at 550 °C (γ phase), and the second one is up to 800 °C (δ phase). Subsequently, the θ and α phase becomes the dominant phase as the temperature increases to 1000 and 1200 °C, respectively.

The specific transition processes are summarized in Table 5. Furthermore, we check the ICP-MS results for one type of

Table 5. Products of the Three Alumina Hydrates under Different Calcination Temperatures

alumina hydrates	300 °C	550 °C	800 °C	1000 °C	1200 °C
bayerite	boehmite + η	η	$\eta + \theta$	$\theta + \alpha$	α
PB	boehmite	γ	δ	θ	α
boehmite	boehmite	γ	δ	θ	α

Table 6. Purity Analysis of α-Al$_2$O$_3$ Obtained at 1200 °C

α-Al$_2$O$_3$	host element content (%)	impurity element content (ppm)				
	Al	Ga	In	Sn	Fe	Na
bayerite-calcined	47.5%	142.3	75.5	65.9	35.5	17.1
PB-calcined	48.8%	151.3	87.1	60.4	17.1	13.3
boehmite-calcined	46.0%	194.8	77.6	53.7	33.0	12.9

prepared derivative (*i.e.*, α-Al$_2$O$_3$). As shown in Table 6, the total impurity element content of each product is less than 450 ppm (especially, the Na impurity is less than 18 ppm and the Fe impurity is less than 36 ppm), which highlights their potentiality in industrial applications.

4. CONCLUSIONS

In this study, a facile temperature-controlled "green" preparation method by the reaction between Al and water was investigated and a series of high-quality hydrated aluminas were obtained. As the temperature increases, the product changes from bayerite (40−50 °C) to PB (70−120 °C) and finally to boehmite (130−160 °C). The reaction mechanism is attributed to the balance of the dissolution and recrystallization processes in the Al−H$_2$O reactions, which can be well controlled by the temperature. Particularly, the obtained products possess high purity (total impurity element content: <450 ppm, impurity Na element content: <21 ppm, and impurity Fe content: <52 ppm) and satisfactory surface properties (specific surface area: 332.7 m^2 g^{-1}, pore volume: 0.3 cm^3 g^{-1}, and pore diameter: 3.6 nm of PB), which has reached the performance standard of commercial PB (SB, produced by Sasol). Since small amounts of contaminating products are used or generated during the whole preparation process, this method is promisingly beneficial to the practical production by increasing the added value of the hydrogen energy industry.

ASSOCIATED CONTENT

Ⓢ Supporting Information

The Supporting Information is available free of charge at https://pubs.acs.org/doi/10.1021/acsomega.2c01543.

Variation of microcrystallite dimension and interplanar crystal spacing (Figure S1); reaction yields at different temperatures (Table S1); ICP analysis of the three prepared alumina hydrates and commercial PB (Table S2); pore property analysis of the samples (Figures S2 and S3); and SEM image of the sample and its calcined product (Figure S4) (PDF)

AUTHOR INFORMATION

Corresponding Author

Shaonan Xu − *Key Laboratory of Automobile Materials of Ministry of Education, Jilin Province Solid Waste Utilization Project Center, Department of Materials Science and Engineering, Jilin University, Changchun 130022 Jilin Prov., China;* ⊙ orcid.org/0000-0002-4510-6728; Email: xsn@jlu.edu.cn

Authors

Wenjing Fu − *Key Laboratory of Automobile Materials of Ministry of Education, Jilin Province Solid Waste Utilization Project Center, Department of Materials Science and Engineering, Jilin University, Changchun 130022 Jilin Prov., China*

Cundi Wei − *Key Laboratory of Automobile Materials of Ministry of Education, Jilin Province Solid Waste Utilization Project Center, Department of Materials Science and Engineering, Jilin University, Changchun 130022 Jilin Prov., China;* ⊙ orcid.org/0000-0001-7411-1844

Jing Zuo − *Key Laboratory of Automobile Materials of Ministry of Education, Jilin Province Solid Waste Utilization Project Center, Department of Materials Science and Engineering, Jilin University, Changchun 130022 Jilin Prov., China*

Jiupeng Zhang − *Key Laboratory of Automobile Materials of Ministry of Education, Jilin Province Solid Waste Utilization Project Center, Department of Materials Science and Engineering, Jilin University, Changchun 130022 Jilin Prov., China*

Jinyi Zhang − *Key Laboratory of Automobile Materials of Ministry of Education, Jilin Province Solid Waste Utilization Project Center, Department of Materials Science and Engineering, Jilin University, Changchun 130022 Jilin Prov., China*

Complete contact information is available at:
https://pubs.acs.org/10.1021/acsomega.2c01543

Notes
The authors declare no competing financial interest.

ACKNOWLEDGMENTS

REFERENCES

(1) Guan, X.; Zhou, Z.; Luo, P.; Wu, F. S.; Dong, S. J. Effects of preparation method on the hydrolytic hydrogen production performance of Al-rich alloys. *J. Alloy Compd.* **2019**, *796*, 210−220.

(2) Huang, T. P.; Gao, Q.; Liu, D.; Xu, S. N.; Guo, C. B.; Zou, J. J.; Wei, C. D. Preparation of Al-Ga-In-Sn-Bi quinary alloy and its hydrogen production via water splitting. *Int. J. Hydrogen Energ.* **2015**, *40*, 2354−2362.

(3) Qiao, D. X.; Lu, Y. P.; Tang, Z. Y.; Fan, X. S.; Wang, T. M.; Li, T. J.; Liaw, P. K. The superior hydrogen-generation performance of multi-component Al alloys by the hydrolysis reaction. *Int. J. Hydrogen Energ.* **2019**, *44*, 3527−3537.

(4) Ilyukhina, A. V.; Kravchenko, O. V.; Bulychev, B. M. Studies on microstructure of activated aluminum and its hydrogen generation properties in aluminum/water reaction. *J. Alloy. Compd.* **2017**, *690*, 321−329.

(5) Wang, W.; Chen, D. M.; Yang, K. Investigation on microstructure and hydrogen generation performance of Al-rich alloys. *Int. J. Hydrogen Energ.* **2010**, *35*, 12011−12019.

(6) Ziebarth, J. T.; Woodall, J. M.; Kramer, R. A.; Choi, G. Liquid phase-enabled reaction of Al—Ga and Al—Ga—In—Sn alloys with water. *Int. J. Hydrogen Energ.* **2011**, *36*, 5271—5279.

(7) Wang, H. Q.; Wang, Z.; Liu, L.; Gong, X. Z.; Wang, M. Y. Alumina hydrate polymorphism control in Al—water reaction crystallization by seeding to change the metastable zone width. *Cryst. Growth Des.* **2016**, *16*, 1056—1062.

(8) Wang, H. Q.; Wang, Z.; Guo, J. W.; Shi, Z. H.; Gong, X. Z.; Cao, J. W. Boehmite preparation via alditols-Interacting transformation of metastable intermediates in Al—H₂O reaction crystallization. *Cryst. Growth Des.* **2017**, *17*, 183—190.

(9) Choi, E.; Song, K.; An, S.; Lee, K.; Youn, M.; Park, K.; Jeong, S.; Kim, H. Cu/ZnO/AlOOH catalyst for methanol synthesis through CO_2 hydrogenation. *Korean J. Chem. Eng.* **2018**, *35*, 73—81.

(10) Li, G. C.; Sun, Y. Y.; Li, X. B.; Liu, Y. Q. Adsorption of congo red from water with spindle-like boehmite: the role of lattice plane (020). *RSC Adv.* **2016**, *6*, 11855—11862.

(11) Jiao, W. Q.; Yue, M. B.; Wang, Y. M.; He, M. Y. Synthesis of morphology-controlled mesoporous transition aluminas derived from the decomposition of alumina hydrates. *Micropor. Mesopor. Mat.* **2012**, *147*, 167—177.

(12) Du, X. L.; Wang, Y. Q.; Su, X. H.; Li, J. G. Influences of pH value on the microstructure and phase transformation of aluminum hydroxide. *Powder Technol.* **2009**, *192*, 40—46.

(13) Fitzgerald, J. J.; Piedra, G.; Dec, S. F.; Seger, M.; Maciel, G. E. Dehydration studies of a high-surface-area alumina (pseudo-boehmite) using solid-state ¹H and ²⁷Al NMR. *J. Am. Chem. Soc.* **1997**, *119*, 7832—7842.

(14) Liu, F. J.; Zuo, S. F.; Xia, X. D.; Sun, J.; Zou, Y. C.; Wang, L.; Li, C. G.; Qi, C. Z. Generalized and high temperature synthesis of a series of crystalline mesoporous metal oxides based nanocomposites with enhanced catalytic activities for benzene combustion. *J. Mater. Chem. A* **2013**, *1*, 4089—4096.

(15) Mi, J.; Chen, X.; Zhang, Q.; Zheng, Y.; Xiao, Y.; Liu, F.; Au, C. T.; Jiang, L. Mechanochemically synthesized MgAl layered double hydroxide nanosheets for efficient catalytic removal of carbonyl sulfide and H_2S. *Chem. Commun.* **2019**, *55*, 9375—9378.

(16) Zhang, X.; Yang, W. W.; Gao, M. Y.; Liu, H.; Li, K. F.; Yu, Y. S. Room-temperature solid phase surface engineering of BiOI sheets stacking g-C₃N₄ boosts photocatalytic reduction of Cr(VI). *Green Energy Environ.* **2022**, *7*, 66—74.

(17) Zhang, X.; Tian, F. Y.; Lan, X.; Liu, Y. Q.; Yang, W. W.; Zhang, J.; Yu, Y. S. Building P-doped MoS₂/g-C₃N₄ layered heterojunction with a dual-internal electric field for efficient photocatalytic sterilization. *Chem. Eng. J.* **2022**, *429*, 132588.

(18) Zhang, X.; Tian, F. Y.; Gao, M. Y.; Yang, W. W.; Yu, Y. S. L-Cysteine capped Mo₂C/Zn₀.₆₇Cd₀.₃₃S heterojunction with intimate covalent bonds enables efficient and stable H₂-Releasing photocatalysis. *Chem. Eng. J.* **2022**, *428*, 132628.

(19) Bao, S. Y.; Wang, Y. J.; Wei, Z. S.; Yang, W. W.; Yu, Y. S. Highly efficient recovery of heavy rare earth elements by using an amino-functionalized magnetic graphene oxide with acid and base resistance. *J. Hazard. Mater.* **2022**, *424*, 127370.

(20) Geng, S.; Tian, F. Y.; Li, M. G.; Liu, Y. Q.; Sheng, J.; Yang, W. W.; Yu, Y. S.; Hou, Y. L. Activating interfacial S sites of MoS₂ boosts hydrogen evolution electrocatalysis. *Nano Res.* **2022**, *15*, 1809—1816.

(21) Zhou, X. D.; Zhang, J.; Ma, Y. M.; Tian, H.; Wang, Y.; Li, Y. G.; Jiang, L. N.; Cui, Q. L. The solvothermal synthesis of γ-AlOOH nanoflakes and their compression behaviors under high pressures. *RSC Adv.* **2017**, *7*, 4904—4911.

(22) Porsin, A. V.; Rogoznikov, V. N.; Kulikov, A. V.; Salanov, A. N.; Serkova, A. N. Crystallization of aluminum hydroxide in a sodium aluminate solution on a heterogeneous surface. *Cryst. Growth Des.* **2017**, *17*, 4730—4738.

(23) de Miranda, L.; Goulart, L. J. P.; de Andrade e Silva, L. G.; Donadon, A. C.; Yamasaki, F. Y.; Munhoz Junior, A. H. Characterization of polystyrene nanocomposites containing nanoparticles of pseudoboehmite obtained by sol-gel process. *J. Nano Res-sw* **2017**, *47*, 96—105.

(24) Qin, Q.; Kim, T.; Duan, X. C.; Lian, J. B.; Zheng, W. J. Novel synthesis strategy of γ-AlOOH nanotubes: coupling reaction via Ionic liquid-assisted hydrothermal route. *Cryst. Growth Des.* **2016**, *16*, 6139—6143.

(25) Cai, W. Q.; Yu, J. G.; Gu, S. H.; Jaroniec, M. Facile hydrothermal synthesis of hierarchical boehmite: sulfate-mediated transformation from nanoflakes to hollow microspheres. *Cryst. Growth Des.* **2010**, *10*, 3977—3982.

(26) Amini, M. M.; Mirzaee, M. Effect of solution chemistry on preparation of boehmite by hydrothermal. *J. Sol-Gel Sci. Techn.* **2005**, *36*, 19—23.

(27) Shen, L.; Hu, C. F.; Sakka, Y.; Huang, Q. Study of phase transformation behaviour of alumina through precipitation method. *J. Phys. D: Appl. Phys.* **2012**, *45*, 215302.

(28) He, T. B.; Xiang, L.; Zhu, S. L. Hydrothermal preparation of boehmite nanorods by selective adsorption of sulfate. *Langmuir* **2008**, *24*, 8284—8289.

(29) Zakharchenya, R. I.; Vasilevskaya, T. N. Influence of hydrolysis temperature on the hydrolysis products of aluminium alkoxides. *J. Mater. Sci.* **1994**, *29*, 2806—2812.

(30) Cocke, D. L.; Johnson, E. D.; Merrill, R. P. Planar models for alumina-based catalysts. *Catal. Rev.* **1984**, *26*, 163—231.

(31) Balan, E.; Blanchard, M.; Hochepied, J.-F.; Lazzeri, M. Surface modes in the infrared spectrum of hydrous minerals: the OH stretching modes of bayerite. *Phys. Chem. Miner.* **2008**, *35*, 279—285.

(32) Nail, S. L.; White, J. L.; Hem, S. L. Comparison of IR spectroscopic analysis and X-Ray diffraction of aluminum hydroxide gel. *J. Pharm. Sci-us* **1975**, *64*, 1166—1169.

(33) Alex, T. C.; Kailath, A. J.; Kumar, R. Al-monohydrate (boehmite) to Al-trihydrate (bayerite/gibbsite) transformation during high-energy milling. *Metall. Mater. Trans. B* **2020**, *51*, 443—451.

(34) Alex, T. C.; Kumar, R.; Roy, S. K.; Mehrotra, S. P. Anomalous reduction in surface area during mechanical activation of boehmite synthesized by thermal decomposition of gibbsite. *Powder Technol.* **2011**, *208*, 128—136.

(35) Pereira Antunes, M. L.; de Souza Santos, H.; de Souza Santos, P. Characterization of the aluminum hydroxide microcrystals formed in some alcohol—water solutions. *Mater. Chem. Phys.* **2002**, *76*, 243—249.

(36) Alwitt, R. S. The growth of hydrous oxide films on aluminum. *J. Electrochem. Soc.* **1974**, *121*, 1322—1328.

(37) Zhang, J.; Klasky, M.; Letellier, B. C. The aluminum chemistry and corrosion in alkaline solutions. *J. Nucl. Mater.* **2009**, *384*, 175—189.

(38) Schoen, R.; Roberson, C. E. Structures of aluminum hydroxide and geochemical implications. *Am. Mineral.* **1970**, *55*, 1—2.

(39) Vedder, W.; Vermilyea, D. A. Aluminum + Water Reaction. *Trans. Faraday Soc.* **1969**, *65*, 561—584.

(40) Hart, R. K. The formation of films on aluminum immersed in water. *Trans. Faraday Soc.* **1957**, *53*, 1020—1027.

(41) Hemingway, S. B. Gibbs free energies of formation for bayerite, nordstrandite, $Al(OH)^{2+}$, and $Al(OH)_2^+$, aluminum mobility, and the formation of bauxites and laterites. In *Springer New York,* 1982; pp. 285—316, DOI: 10.1007/978-1-4612-5683-0_9.

(42) Aldcroft, D.; Bye, G. C.; Hughes, C. A. Crystallisation processes in aluminium hydroxide gels. *J. Appl. Chem.* **1964**, *19*, 167—172.

(43) Digne, M.; Sautet, P.; Raybaud, P.; Toulhoat, H.; Artacho, E. Structure and stability of aluminum hydroxides: a theoretical study. *J. Phys. Chem. B* **2002**, *106*, 5155—5162.

(44) Wang, W.; Zhao, X. M.; Chen, D. M.; Yang, K. Insight into the reactivity of Al—Ga—In—Sn alloy with water. *Int. J. Hydrogen Energ.* **2012**, *37*, 2187—2194.

(45) Ilyukhina, A. V.; Ilyukhin, A. S.; Shkolnikov, E. I. Hydrogen generation from water by means of activated aluminum. *Int. J. Hydrogen Energ.* **2012**, *37*, 16382—16387.

(46) Gao, J. F.; Xu, C. Y.; Wang, J. Z.; Wang, J. F.; Zhuang, Y. Y. Preparation of ultra-pure pseudo-boehmite from sodium meta-aluminate. *Chin. J. Catal.* **2003**, *24*, 505—508.

(47) Hind, A. R.; Bhargava, S. K.; Grocott, S. C. The surface chemistry of Bayer process solids: a review. *Colloids Surf., A* **1999**, *146*, 359—374.

(48) Zhang, Z.; Pinnavaia, T. J. Mesoporous gamma-alumina formed through the surfactant-mediated scaffolding of peptized pseudoboehmite nanoparticles. *Langmuir* **2010**, *26*, 10063−10067.

(49) Yang, F.; Wang, Q.; Yan, J. L.; Fang, J.; Zhao, J. H.; Shen, W. G. Preparation of high pore volume pseudoboehmite doped with transition metal ions through direct precipitation method. *Ind. Eng. Chem. Res.* **2012**, *51*, 15386−15392.

(50) Liu, F. J.; Liu, C. L.; Hu, B. W.; Kong, W. P.; Qi, C. Z. High-temperature hydrothermal synthesis of crystalline mesoporous TiO$_2$ with superior photo catalytic activities. *Appl. Surf. Sci.* **2012**, *258*, 7448−7454.

(51) Yang, Y.; Xu, Y.; Han, B.; Xu, B.; Liu, X.; Yan, Z. Effects of synthetic conditions on the textural structure of pseudo-boehmite. *J. Colloid Interface Sci.* **2016**, *469*, 1−7.

(52) Cai, W. Q.; Li, H. Q.; Zhang, Y. Influences of processing techniques of the H$_2$O$_2$-precipitated pseudoboehmite on the structural and textural properties of γ-Al$_2$O$_3$. *Colloids Surf, A* **2007**, *295*, 185−192.

(53) Wang, K.; Yang, W. J.; Gao, X. J.; Wang, X. T. Effect of preparation conditions on crystal size and pore structure of pseudoboehmite. *J. Tianjin Univ.* **2013**, *46*, 934−938.

(54) Qu, L. H.; He, C. Q.; Yang, Y.; He, Y. L.; Liu, Z. M. Hydrothermal synthesis of alumina nanotubes templated by anionic surfactant. *Mater. Lett.* **2005**, *59*, 4034−4037.

(55) Yan, Y. F.; Zhi, J. P.; Zhang, G. Y. Influence of successive washing on porous structure of pseudoboehmite. *J. Nat. Gas Chem.* **2005**, *14*, 181−188.

(56) Ren, T. Z.; Yuan, Z. Y.; Su, B. L. Microwave-assisted preparation of hierarchical mesoporous-macroporous boehmite AlOOH and γ-Al$_2$O$_3$. *Langmuir* **2004**, *20*, 1531−1534.

(57) Wang, Y. Y.; Zhao, C. W.; He, J. S.; Yan, Y.; Zhang, X. L.; Luan, Z. K. Preparation of pseudo-boehmite and γ-Al$_2$O$_3$ by polyaluminum chloride II-surfactant influences. *Chin. J. Inorg. Chem.* **2012**, *28*, 302−306. http://ir.rcees.ac.cn/handle/311016/8420

(58) Toledo-Chávez, G.; Paniagua-Rodríguez, J.-C.; Zárate-Medina, J.; Maya-Yescas, R. Reactions analysis during the synthesis of pseudo-boehmite as precursor of gamma-alumina. *Catal. Today* **2016**, *271*, 207−212.

(59) Guzmán-Castillo, M. L.; Bokhimi, X.; Toledo-Antonio, A.; Salmones-Blásquez, J.; Hernández-Beltrán, F. Effect of boehmite crystallite size and steaming on alumina properties. *J. Phys. Chem. B* **2001**, *105*, 2099−2106.